Light Metals 2014
Edited by: John Grandfield
TMS (The Minerals, Metals & Materials Society), 2014

CURRENT EFFICIENCY IN ALUMINIUM REDUCTION CELLS: THEORIES, MODELS, CONCEPTS, AND SPECULATIONS

Asbjørn Solheim

SINTEF Materials and Chemistry
P.O. Box 4760 Sluppen, NO-7465 Trondheim, Norway

Keywords: Current efficiency; dissolved metal; electronic conductivity

Abstract

Some theories and concepts regarding current efficiency (CE) in aluminium reduction cells are reviewed. The Sterten-Solli model, which represents the current understanding, explains the CE loss as a result of the formation of dissolved metal at the cathode, notably sodium. Sodium is transported into the electrolyte across the boundary layer at the cathode, "stealing" electrons that would otherwise be used in the main cathode reaction. While dissolved species may be transported by ordinary mass transfer; it is also known that cryolitic melts containing dissolved metal exhibit electronic conductivity. The main content in the present paper is an attempt to separate between CE loss by ordinary mass transfer and CE loss by electronic conduction, and to explain the relationship between the two. This constitutes the basis for a new "integrated" CE model, which apparently implies a weaker relationship between CE and convection than what can be calculated by ordinary mass transfer.

Introduction

The current efficiency in the Hall-Héroult process has increased steadily since the invention of the process in 1886. The present state-of-the-art technologies boast CEs of 92-95 percent and even higher. It is generally agreed that the increased CE is owed to process improvements such as magnetic compensation, point feeders, automatic cell control, and improved electrolyte (bath) chemistry.

A large amount of work has been devoted to understanding the mechanisms behind the loss in CE. Comprehensive reviews of the effect of different parameters on the CE in laboratory cells as well as in industrial cells have been published by Grjotheim *et al*. [1], Kvande [2], and Thonstad *et al*. [3]. Still, the underlying mechanisms are not very clearly understood and partly disputed.

The purpose of the present work is to present some important concepts and theories concerning CE during normal electrolysis as well as at small anode-cathode distance. Furthermore, some new ideas are forwarded concerning the possibility of deriving an "integrated" current efficiency model based on electronic conduction in combination with diffusion in a boundary layer.

Loss in Current Efficiency: General Descriptions

Theoretical Yield

The theoretical yield in any electrolysis process is given by the well-known Faraday's law,

$$N = \frac{I \cdot t}{n F} \quad [\text{mole}] \tag{1}$$

where N is the number of moles produced, I is the current [A], t is time [s], n is the number of electrons supplied per atom or molecule of the product (3 for aluminium), and F is Faraday's constant [96485 As · equiv^{-1}]. From this equation it can easily be calculated that the theoretical aluminium production in a 300 kA cell is 2416 kg/day. The CE is defined as the ratio between the real production and this theoretical amount. It is generally agreed that the main part of the loss in CE can be attributed to loss of dissolved metal from the cathode into the bath.

In the following, it is implicitly assumed that the bulk of electrolyte does not contain metal droplets or gas bubbles.

Traditional Description of Loss in Current Efficiency

In the traditional description of loss in CE, it is assumed that Al is formed in the main reaction. A part of the product dissolves in the electrolyte and becomes re-oxidised in the "back reaction",

$$\text{Main reaction}: \quad \tfrac{1}{2}Al_2O_3 + \tfrac{3}{4}C = Al + \tfrac{3}{4}CO_2 \tag{2}$$

$$\text{Back reaction}: \quad Al + \tfrac{3}{2}CO_2 = \tfrac{1}{2}Al_2O_3 + \tfrac{3}{2}CO \tag{3}$$

The total turnover in the cell is calculated by multiplying Equation (3) by (1-ε) where ε is the fractional current efficiency (*e.g.*, ε = 0.94) and adding the result to the main reaction (2),

$$\tfrac{\varepsilon}{2}Al_2O_3 + \tfrac{3}{4}C = \varepsilon Al + \tfrac{3}{4}(2\varepsilon - 1)CO_2 + \tfrac{3}{2}(1-\varepsilon)CO \tag{4}$$

Although the total turnover described by Equation (4) is correct, the treatment is problematic. Firstly, dissolved Al (as such) does not exist in the electrolyte (see the next section). Secondly, Eqs. (2) and (3) in fact imply that all electrons are first being used for producing aluminium at the cathode, which is highly unlikely. The description is easy to comprehend, but it is simplistic and not suited for a detailed theoretical treatment of the loss mechanisms.

Dissolved Metal

It is well known that many metals dissolve in their halides [4]. The electrolyte in the Hall-Héroult process contains mainly NaF and AlF_3, and the following equilibrium exists at the cathode

$$Al + 3NaF = 3Na + AlF_3 \tag{5}$$

Therefore, as would be expected, the electrolyte contains dissolved metal in the form of sodium as well as aluminium

species. Work by Ødegård *et al*. [5] and Wang *et al*. [6] show that dissolved metal consists of Na and a number of aluminium-containing species with reduced valence, *e.g*., AlF_2^- where Al is monovalent [5], in amounts corresponding to about 0.1 wt% "dissolved Al". Dissolved alkali metals often give rise to electronic conductivity, and it has been shown that cryolitic melts containing dissolved metal has electronic conductivity [7, 8], which must be attributed to dissolved Na. The subvalent aluminium species probably behave just like other anions present in the melt.

Modern Description of Loss in Current Efficiency

The main electrode reactions in a Hall-Heroult are as follows,

Cathode reaction:

$$AlF_3 + 3Na^+ + 3e \rightarrow Al + 3\,NaF \qquad (6)$$

Anode reaction:

$$\tfrac{1}{2}Al_2O_3 + \tfrac{3}{4}C + 3NaF \rightarrow AlF_3 + \tfrac{3}{4}CO_2 + 3Na^+ + 3e \qquad (7)$$

The total cell reaction is the sum of the two electrode reactions (see Equation (2)). "AlF_3" represents the core of Al-containing complexes such as AlF_4^-, AlF_6^{3-}, *etc*.

In the modern description of CE in aluminium cells, the fractional current efficiency is related directly to the electric current (I),

$$\varepsilon = I_{Al}/I_{tot} = 1 - I_{loss}/I_{tot} \qquad (8)$$

where I_{Al} is related to reaction (6) and I_{loss} is attributed to parasitic side reactions. Due to its "electronic properties", Na is probably the more important part of the dissolved metal due to the high mobility of the associated electrons. Formation of dissolved metal "steals" electrons that would otherwise be used for producing Al. Formulated with 3 electrons,

$$3\,Na^+ + 3e = 3\,Na_{diss} \qquad (9)$$

The dissolved sodium diffuses away from the cathode, and is transported to the reaction site. Thereafter, it is oxidised by the anode gas (or by the anode itself),

$$3\,Na_{diss} + \tfrac{3}{2}CO_2 + AlF_3 = 3\,NaF + \tfrac{1}{2}Al_2O_3 + \tfrac{3}{2}CO \qquad (10)$$

The total side reaction then becomes the sum of Eqs. (9) and (10),

$$3\,Na^+ + 3e + \tfrac{3}{2}CO_2 + AlF_3 = 3\,NaF + \tfrac{1}{2}Al_2O_3 + \tfrac{3}{2}CO \qquad (11)$$

The total turnover in the cell can now be found by multiplying the main cathode reaction (6) by ε and the parasitic reaction (11) by (1-ε) and adding the result to the anode reaction (7). The result is identical with Equation (4).

Equation (10) can be apprehended as a form of the "back reaction", Equation (3). However, since Equation (3) refers to re-oxidation of already formed aluminium, it is the author's opinion that "side reaction" or "parasitic reaction" is a better term.

Similar reactions can be formulated for subvalent aluminium species. Electrochemical reactions proceed in steps, and subvalent aluminium can be regarded as intermediate products that escape from the cathode,

$$AlF_3 + 2e = AlF_2^- + F^- \qquad (12)$$

Dissolved aluminium and dissolved sodium will also be at equilibrium at any point,

$$AlF_2^- + 2\,NaF = 2\,Na + AlF_3 + F^- \qquad (13)$$

Rate-limiting steps. Reaction Site

CO_2 evolved at the anode is soluble in the bath. Provided that dissolved metal and CO_2 do not co-exist, and that the mass transfer resistance in the bulk of the bath is negligible due to turbulence, the reaction between dissolved metal and CO_2 takes place either close to the bubble or close to the cathode. There are four possible rate-limiting steps depending on mass transfer coefficients and solubilities, as illustrated in Figure 1. Taking Case III as an example, when $k_cA_c/k_bA_b << 1$ (product of mass transfer coefficient and interfacial area of the cathode and the gas bubbles, respectively), transport through the cathode boundary layer will be slow and hence rate-determining (*i.e*., changes at the cathode are more important than changes at the anode). If the solubility of CO_2 (c_g^{sat}) is much higher than the solubility of metal, the bulk of the bath contains CO_2 rather than dissolved metal, and the reaction site will be located inside the cathode boundary layer. A more detailed treatment is given by Lillebuen and Mellerud [9].

Solheim and Thonstad [10] carried out experiments concerning the mass transfer coefficient at the gas phase in a water model. It was concluded that the mass transfer coefficient at the bubbles will be about $2 \cdot 10^{-4}$ ms^{-1} (referred to the anode surface area) for a species with diffusion coefficient $D = 1 \cdot 10^{-9}$ m^{2}s^{-1}. This is one order of magnitude higher than the mass transfer coefficient at the cathode, as derived by Jentoftsen [11].

The solubility of dissolved metal appears to be in the order of 10^2 equiv/m^3. This can be compared with the solubility of CO_2, which is one order of magnitude lower (*e.g*., 8 equiv/m^3 in a melt with NaF/AlF_3 ratio of 2.3 containing 5.33 wt% Al_2O_3 at 1000 °C [12].

The above order-of-magnitude considerations indicate that the reaction site is close to the gas bubbles and that transport of dissolved metal across the cathode boundary layer is the rate-limiting step (Case I in Figure 1).

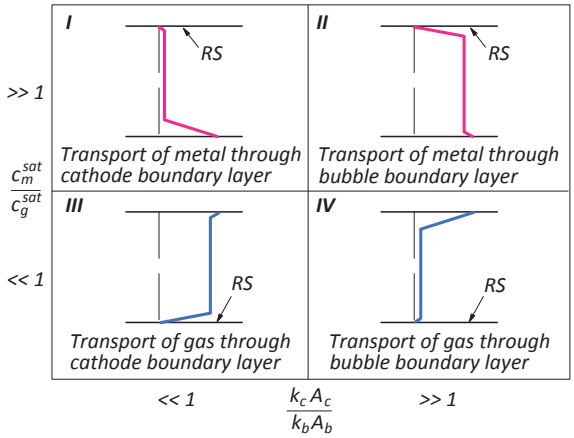

Figure 1. Concentration profiles of dissolved metal (Cases I and II) and dissolved CO_2 (Cases III and IV) at different conditions. RS – reaction site. The rate-limiting step is indicated (see text).

The Sterten-Solli Model

The following considerations are the basis of the Sterten-Solli current efficiency model [13, 14],

- The rate-determining step is at the cathode boundary layer.
- The loss in CE is explained by parasitic side reactions leading to transport of electrons away from the cathode. The electrons are (somehow) related to the activity of dissolved sodium.
- The activity of sodium at the cathode depends on the equilibrium shown in Equation (5). The activities of NaF and AlF_3 depend on the cathodic concentration overvoltage, which must also be taken into consideration.

The final model was expressed by [14]

$$i_{loss} = F k_{mix} a_{Na(eq)}^{y} \left(\exp\left\{ \frac{-F\eta y}{RT} \right\} - \alpha^{y} \right) \qquad (14)$$

where i_{loss} is the loss current density (parasitic side reactions), k_{mix} is a "mixed" mass transfer coefficient (or rate constant), $a_{Na(eq)}$ is the equilibrium sodium activity in a melt with bulk properties, y is an empirical sodium activity exponent, η is the cathodic concentration overvoltage, and α is the ratio between the real sodium activity in the bulk and at equilibrium.

Based on comparison with experimental data, the exponent y was found to be close to 0.5 [15]; *i.e.*, the loss in CE is near proportional to the square root of the activity of sodium. The Sterten-Solli model does not distinguish explicitly between electronic conduction and chemical diffusion, but it should be noted that the "mass transfer coefficient" k_{mix} is a lumped parameter that comprises all kind of transport mechanisms, not only ordinary mass transfer. The model gives an excellent fit to laboratory experimental data, but it has not been possible to study systematically how k_{mix} (or i_{loss}) depends on convection.

Outline of an "Integrated" Current Efficiency Model

The term "integrated model" refers to a CE model where the effects of ordinary mass transfer and electronic conduction are separated and taken into account explicitly. In the Sterten-Solli model, the mechanisms are combined and expressed by a single variable (k_{mix}). The two mechanisms can be related as illustrated in Figure 2. In the "diffusion" point of view, dissolved Na must be assigned a very high diffusion coefficient, due to the high mobility of electrons. Although the two viewpoints apparently give the same result, it is likely that the effect of convection is different in the two types of transport mechanisms, and this is the main motivation for the treatment in the following.

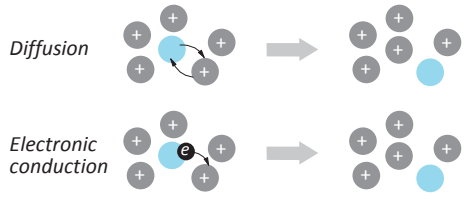

Figure 2. Schematic illustration of transport of dissolved metal through a lattice of Na^+ and anions (not shown). Na may be transported by diffusion (Na and Na^+ change positions) or by electronic conduction (an electron moves from Na to a neighbouring Na^+). In both cases, dissolved Na moves one position towards right.

Electronic Conduction and Loss in Current Efficiency

The equilibrium shown in Equation (5) implies that the activities of dissolved Na, NaF, and AlF_3 can be described by

$$a_{Na} \propto a_{NaF} \cdot a_{AlF_3}^{-1/3} \qquad (15)$$

Dissolved Na can be apprehended as a sodium cation surrounded by a more or less loosely associated electron. We assume that neutral (metallic) Na takes an interstitial position in the lattice, and that it is at equilibrium with interstitial Na cations and "free" electrons. In Kröger-Vink notation,

$$Na_i^{\times} = Na_i^{\bullet} + e' \qquad (16)$$

The concentrations of the two species on the right hand side are equal. Assuming proportionality between concentration and activity, we obtain

$$c_{e'} \cdot c_{Na_i^{\bullet}} \propto a_{Na_i^{\times}} \Rightarrow c_{e'} \propto \sqrt{a_{Na_i^{x}}} \qquad (17)$$

This means that we should expect that the electronic conductivity (κ_e) is proportional with the square root of the sodium activity,

$$\kappa_e \propto \sqrt{a_{Na}} \propto a_{NaF}^{1/2} \cdot a_{AlF_3}^{-1/6} \qquad (18)$$

This seems indeed to be true for the data published by Haarberg *et al.* [7]. Their data can be well fitted by

$$\kappa_e = 1.53 \cdot 10^{11} \cdot \exp\left(\frac{-233500}{RT} \right) \cdot a_{NaF}^{1/2} \cdot a_{AlF_3}^{-1/6} \qquad (19)$$

where κ_e is the electronic conductivity in Sm^{-1} and the activities of NaF and AlF_3 at alumina saturation was computed from the activity model by Solheim and Sterten [15]. A graphic representation of the data is shown in Figure 3.

Solli *et al.* [14] measured the CE as a function of the NaF/AlF_3 molar ratio. These data can also be well represented assuming that the loss in CE is proportional with the square root of the sodium activity (Figure 4).

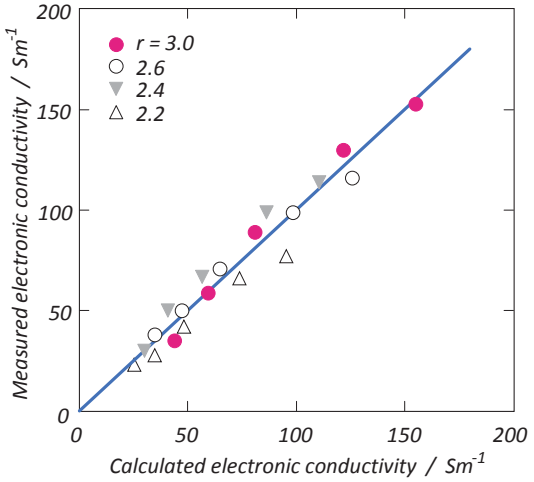

Figure 3. Electronic conductivity in cryolitic melts. Comparison between Equation (19) and experimental data by Haarberg *et al.* [7] in alumina-saturated melts with different NaF/AlF_3 molar ratios (r) and temperatures.

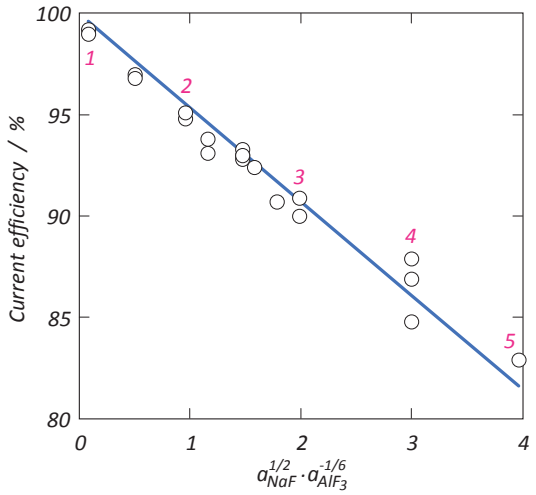

Figure 4. Current efficiency in a laboratory cell [14] as a function of the square root of the sodium activity in the system NaF-AlF_3 [15]. The numbers in the figure represent the NaF/AlF_3 molar ratio in the experiments. No attempts were made to correct for the change in NaF/AlF_3 ratio through the cathodic boundary layer.

Preliminary Formulation of Model

A very preliminary description of the integrated current efficiency model is outlined in the following. The model is based on the following assumptions,

1. Only dissolved Na and $NaAlF_2$ are taken into account.
2. Dissolved Na and $NaAlF_2$ are at equilibrium throughout the boundary layer (Equation (13)).
3. The total loss current density (i_{loss}) is separated into an electronic contribution (i_e) and a mass transport contribution (i_c). The sum of i_e and i_c is constant throughout the cathode boundary layer to avoid accumulation of charges.
4. The local electronic contribution i_c is proportional with the square root of the local sodium concentration (Equation (18).
5. The mass transport contribution i_c is related to the molar flux of $NaAlF_2$ (ordinary mass transport of Na is not taken into account at the present stage).
6. The concentration of dissolved sodium is negligible in the bulk of the bath. Hence, the electronic conductivity decreases throughout the cathode boundary layer.
7. Variation in the activities of NaF and AlF_3 across the cathode boundary layer is not taken into account at the present stage.
8. Ordinary mass transport ($NaAlF_2$) is calculated based on a turbulent diffusion coefficient which is proportional with y^3 where y is the distance from the cathode. This is further explained elsewhere [16].

Simplified Computational Procedure

Since the bath is a multicomponent mixture where all substances are involved in diffusion at the cathode, a strict treatment must involve the Stefan-Maxwell equations. However, the assumptions 5 and 7 in the preceding section allows for a simplified treatment. In this treatment, the electronic current density i_e at the cathode is fixed. The vicinity of the cathode is divided into a number of elements with height Δy = 0.015 mm. The mass transport contribution i_c due to diffusion of $NaAlF_2$ at the cathode (element no. 1) is chosen initially. From this value, the concentration of $NaAlF_2$ in element no. 2 is calculated,

$$c_{NaAlF_2(2)} = c_{NaAlF_2(1)} - \frac{i_{c(1)}}{2F} \cdot \frac{\Delta y}{D_c + D_{t(1)}} \qquad (20)$$

where D_c is the chemical diffusion coefficient for $NaAlF_2$ and D_t is the turbulent diffusion coefficient. The latter was calculated by $D_t = Cy^3$, and it can be shown [16] that the mass transfer coefficient (k) is given by

$$k = 0.8270\, D_c^{2/3} \cdot C^{1/3} \qquad (21)$$

The concentration of sodium in element no. 2 is calculated according to the equilibrium in Equation (13),

$$c_{Na(2)} = c_{Na(1)} \cdot \sqrt{\frac{c_{NaAlF_{2(2)}}}{c_{NaAlF_{2(1)}}}} \qquad (22)$$

and, in accordance with Equation (19), the electronic current density in element no. 2 becomes

$$i_{e(2)} = i_{e(2)} \cdot \sqrt{\frac{c_{Na(2)}}{c_{Na(1)}}} \qquad (23)$$

Since the total loss current density $i_{loss} = i_e + i_c$ is constant, the diffusional loss in current density in element no. 2 becomes

$$i_{c(2)} = i_{c(1)} + i_{e(1)} - i_{e(2)} \qquad (24)$$

$i_{c(2)}$ is used in the above procedure for calculating the values in element 3, *etc*. The calculation is repeated with new values of i_c in element no. 1 until the concentrations of $NaAlF_2$ and Na are zero far from the cathode (in this case, at y = 10 mm).

Preliminary Results

The above procedure was applied for a case where the actual cathodic current density was 8000 Am^{-2}, the loss density at the cathode due to electronic conduction $i_{e(1)}$ = 350 Am^{-2}, the chemical diffusion coefficient for $NaAlF_2$ $D_c = 3 \cdot 10^{-9}$ m^2s^{-1}, and the concentration of $NaAlF_2$ at the cathode was assumed to be 30 $molm^{-3}$ (this value corresponds to approximately 0.04 wt% "dissolved aluminium").

Figure 5 shows the concentration gradients of Na and $NaAlF_2$ and the distribution between electronic loss current density and diffusional loss current density as a function of the distance from the cathode. As can be observed, the electronic contribution decreases with increasing distance from the cathode, while the diffusional contribution increases. The total loss current density is 487 Am^{-2}, corresponding to CE = 93.91 %.

A series of calculations were made with different mass transfer coefficient for $NaAlF_2$. The result is shown in Figure 6. As can be observed, the current efficiency is a weaker function of the mass transfer coefficient than what would be the case in a purely mass transfer controlled process.

Current Efficiency at Short Anode-Cathode Distance

Most major aluminium companies carry out projects for increasing the amperage and/or decreasing the specific energy consumption. In both cases, the anode-cathode distance (ACD)

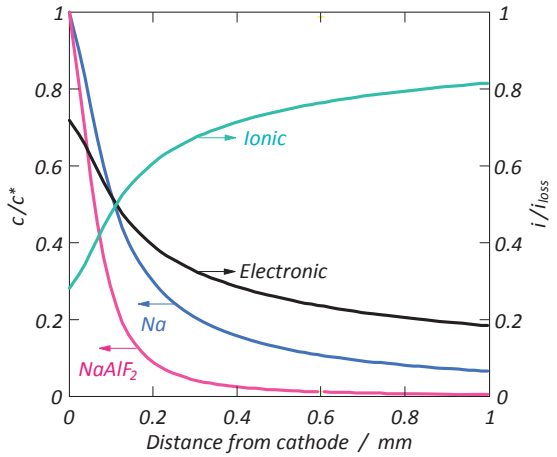

Figure 5. Relative concentrations for Na and $NaAlF_2$ (left hand scale) and relative values for the two CE loss contributions (right hand scale) as a function of the distance from the cathode.

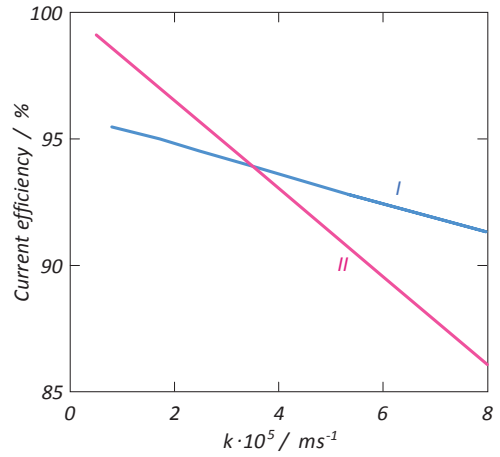

Figure 6. Current efficiency as a function of the mass transfer coeffient for $NaAlF_2$. Curve I – calculated from the present preliminary "integrated" model, curve II – loss in CE due to ordinary mass transfer only.

will have to be reduced. Most studies on CE as a function of ACD in industrial cells show that the CE stays more or less constant until the ACD is lower than a certain critical limit [1]. Some measurements are shown in Figure 7.

The mass transfer coefficient at the cathode depends on convection leading to shear forces at the metal-bath interface. The convection may be caused by magnetohydrodynamic (MHD) flow, or by the turbulence associated with gas bubbles at the anode. The latter becomes particularly important at low ACD. It has been shown that the height of the metal waves increased with decreasing ACD in an industrial cell [17].

The effect of gas bubbles on the mass transfer coefficient at the cathode was studied in a water model by an electrochemical technique. The "bath" contained small amounts of potassium ferricyanide $K_3Fe(CN)_6$ (0.001 M) and potassium ferrocyanide $K_4Fe(CN)_6$ (0.01 M) in 0.5 M NaCl. The "anode" was made of porous bronze. The length of the "anode" (in the direction of the bubble motion) was 0.78 m, and it had an angle of 2.1° *vs.* the horizontal. The cell was also equipped with three 50 x 50 mm nickel plates recessed into the PMMA (Plexiglas) bottom of the model. A DC voltage was applied between the anode and the nickel plates, leading to the following reaction at the nickel plates

$$Fe(CN)_6^{3-} + e \rightarrow Fe(CN)_6^{4-} \qquad (25)$$

The concentration of ferricyanide is low, and the reaction takes place at the limiting current density (i_{lim}). The limiting current density is related to the mass transfer coefficient (k) by

$$k = \frac{i_{lim}}{c\,F} \qquad (26)$$

This means that the recorded current at the nickel electrodes is a direct measure of the mass transfer coefficient.

Some results are shown in Figure 8. As can be observed, the mass transfer coefficient (given as limiting current) increased with decreasing ACD and with increasing gas flow rate (simulated current density). It should be noted that there is no "threshold" or "critical ACD" where the limiting current increases abruptly, nor a region at high ACD where the mass transfer coefficient is independent of ACD. Possibly, this can be taken as an indication that the loss in CE is less than proportional with the mass transfer coefficient, as indicated by curve I in Figure 6. Since the results were obtained in a model with solid bottom, the results will, or course, be more relevant for cells equipped with drained cathodes.

To the present author it seems that the sharp decrease in CE at low ACD must have other explanations than just an increase in the mass transfer coefficient. It was shown by Rolseth *et al.* [17] that the amplitude of the metal waves increased as the ACD was reduced. It is also known that gas bubbles travelling along the anode have thick fronts at and thinner trailing parts ("Fortin bubbles" [18]). The position of the metal as well as the position of the bubble fronts will have an average value and a certain frequency distribution around the average (not necessarily normal distributions as illustrated in Figure 9). Upon decreasing the ACD (and, thereby, increasing amplitude of the metal waves) the highest metal waves and the thickest bubbles will sooner or later collide, and it can easily be imagined that each contact gives a relatively high metal loss. If each collision gives a constant metal loss, the extra loss in CE will be proportional with the area of the overlapping distribution curves illustrated in Figure 9 b). This area increases rapidly when the ACD continues to decrease.

Concluding Remarks

The "integrated" current efficiency model as outlined in the present paper is in no way proved experimentally, and the theory is presently underdeveloped. A logical next step will be taking into the account the diffusion of Na (not only $NaAlF_2$) as well as the bath components NaF and AlF_3. Although precise calculations of the CE will be difficult due to lack of primary data concerning diffusion coefficients and concentrations of the different dissolved metal species, it may be possible to calibrate the model with different kind of experimental data.

Acknowledgement

The work behind the present paper has been going on for several years, and it has been partly financed by Hydro. Permission to publish the result is gratefully acknowledged.

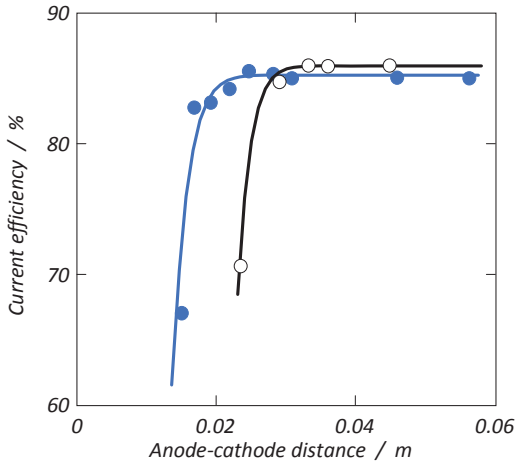

Figure 7. Current efficiency as a function of the anode-cathode distance in an industrial cell (same anode, two consequtive days). Data taken from Rolseth *et al.* [17].

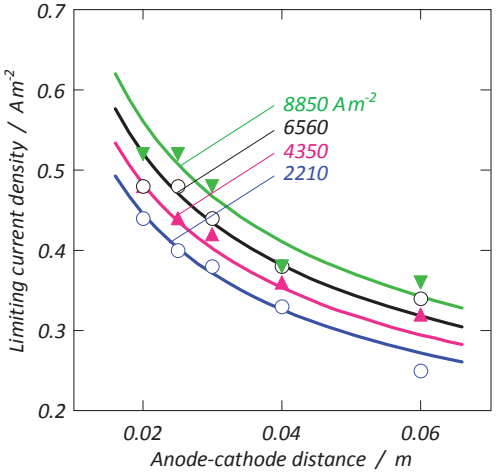

Figure 8. Average limiting current density as a function of the anode-cathode distance at three nickel electrodes placed at the bottom of a water model representing an aluminium cell. The numbers represent simulated current density (gas flow rate).

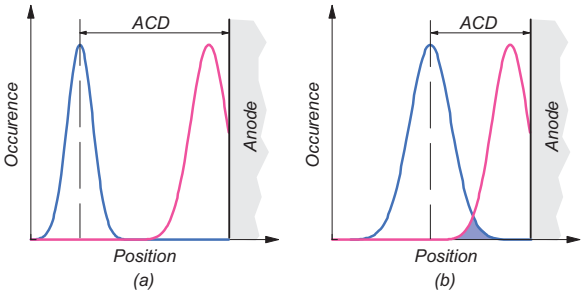

Figure 9. Illustration of overlapping metal wave crests and gas bubble fronts at low ACD, leading to excessive loss is current efficiency.

References

1. K. Grjotheim, C. Krohn, M. Malinovský, K. Matiašovský, and J. Thonstad, Aluminium Electrolysis, Aluminium-Verlag (1st Edition 1977, 2nd Edition 1982).
2. J. Thonstad, P. Fellner, G.M. Haarberg, Ján Híveš, H. Kvande, and Å. Sterten, Aluminium Electrolysis, Aluminium-Verlag (3rd Edition 2001).
3. H. Kvande, "Current Efficiency of Alumina Reduction Cells", Light Metals 1989, pp. 261/68.
4. M.A. Bredig, in M. Blander (Ed.), Molten Salt Chemistry, Interscience, 1964.
5. R. Ødegård, Å. Sterten, and J. Thonstad, "The Solubility of Aluminium in Cryolitic Melts", Light Metals 1987, pp. 389/98.
6. X. Wang, R.D. Peterson, N.E. Richards, "Dissolved Metals in Cryolitic Melts", Light Metals 1991, pp. 323/30.
7. G.M. Haarberg, J. Thonstad, J.J. Egan, R. Oblakowski, and S. Pietrzyk, "Electrical Conductivity Measurements in Cryolite Alumina Melts in the Presence of Aluminium", Light Metals 1996, pp. 221/25.
8. G.M. Haarberg, K.S. Osen, J. Thonstad, R.J. Heus, and J.J. Egan, "Measurement of Electronic Conduction in Cryolite-Alumina Melts and Estimation of Its Effect on Current Efficiency", Light Metals 1991, pp. 283/88.
9. B. Lillebuen and T. Mellerud, "Current Efficiency and Alumina Distribution". Light Metals 1985, pp. 637/46.
10. A. Solheim and J. Thonstad, "Model Experiments of Mass Transfer at the Electrolyte-Gas Interface in Aluminium Cells", Light Metals 1987, pp.239/45.
11. T.E. Jentoftsen, "Behaviour of Iron and Titanium Species in Cryolite-Alumina Melts", Dr.ingeniøravhandling 2000:118, NTNU, 2000.
12. H. Numata and J.O'M. Bockris, "Interactions of Gases in Molten Salts: Carbon Dioxide and Oxygen in Cryolite Alumina Melts", *Met. Trans. B*, **15B**, 36/41 (1984).
13. Å. Sterten and P.A. Solli, "An Electrochemical Current Efficiency Model for Aluminium Electrolysis Cells", *J. Appl. Electrochem.* **26** 187/93 (1996).
14. P.A. Solli, T. Eggen, E. Skybakmoen, and Å. Sterten, "Current Efficiency in Hall-Héroult Cells: Experimental and Modelling Studies", ", *J. Appl. Electrochem.* **27** 939/46 (1997).
15. A. Solheim and Å. Sterten, "Activity of Alumina in the System NaF-AlF_3-Al_2O_3 at NaF/AlF_3 Molar Ratios Ranging from 1.4 to 3", Light Metals 1999, pp. 445/52.
16. A. Solheim, "Some Aspects of Heat Transfer between Bath and Sideledge in Aluminium Reduction Cells", Light Metals 2011, pp. 381/86.
17. S. Rolseth, T. Muftuoglu, A. Solheim, and J. Thonstad, "Current Efficiency at Short Anode-Cathode Distance in Aluminium Electrolysis", Light Metals 1986, pp.517/23.
18. S. Fortin, M. Gerhardt, and J. A. Gesing, "Physical Modelling of Bubble Behaviour and Gas Release from Aluminum Reduction Cell Anodes", Light Metals 1984, pp. 721/41.